Nanoscale

COMMUNICATION

View Article Online
View Journal | View Issue

Cite this: *Nanoscale*, 2018, **10**, 20126

Received 22nd June 2018,
Accepted 21st October 2018

DOI: 10.1039/c8nr05061a

rsc.li/nanoscale

An acidic pH/reduction dual-stimuli responsive nanoprobe for enhanced CT imaging of tumours *in vivo*†

Anna Wang,‡[a] Ling Yin,‡[b,c] Lei He,[a] Huawei Xia,[a] Fei Chen,[d] Meng Zhao,[a] Jianan Ding[a] and Haibin Shi *[a]

Computed tomography (CT) is one of the most frequently used diagnostic imaging modalities in clinics. However, the fast clearance of CT contrast agents through the kidney and short circulation time severely restrict their *in vivo* applications. Herein, taking advantage of the biocompatible CBT condensation reaction, we rationally designed and synthesized a new smart acidic pH/glutathione (GSH) dual-stimuli responsive nanoprobe (1) which can intermolecularly undergo condensation and form a nanoparticle assembly (I-NPs) in the tumour microenvironment. *In vivo* CT imaging results indicated that probe 1 could be successfully applied for enhanced CT imaging of tumours in nude mice with a low dose of 21.79 mg I per kg body weight, which may offer a promising tool for precise tumor diagnosis.

As a growing biomedical discipline, molecular imaging provides an effective means to enable the visualization of the cellular function and uncover the mechanism of physiological and pathological processes such as cancer,[1] cerebral disease,[2] cardiovascular disease,[3] *etc*. To date, many types of imaging technologies, such as ultrasound, positron emission tomography, computed tomography, single photon emission tomography, optical imaging, and magnetic resonance imaging,[4] have been widely applied in biomedical research and clinical diagnosis. Among them, CT has been acknowledged as one of the clinically most important and frequently used medical imaging modalities owing to its high resolution, deep tissue penetration, low cost, and wide availability.[5] Despite CT plays a key role in the clinical diagnosis of diseases, its limited spatial resolution for soft tissues often hampers its broad applications in clinics. Recently, a variety of CT contrast agents have been developed to selectively enhance the contrast between targeted soft tissue and the surrounding tissue for better visualization of pathological regions.[6] Iodinated small molecules such as iohexol, iopamidol and iopromide are typically used as clinical CT contrast agents for disease diagnosis.[7] Nevertheless, there still remain several problems such as rapid blood clearance, high-dose requirement, probable iodine hypersensitivity, and contrast-induced nephropathy, which severely impede their clinical applications.[8] To address these limitations, great efforts have recently been made to develop new CT contrast agents with long blood circulation, low renal clearance rate and capillary leakage. For example, there has been a considerable increase of interest in the use of iodinated organic nanoparticles such as nanoemulsions,[9] liposomes,[10] dendrimers,[11] and inorganic nanoparticles (*e.g.*, gold,[12] tantalum,[13] lanthanum,[14] and bismuth[15]) as CT contrast agents for tumour imaging. Unfortunately, these nano-sized CT contrast agents encounter the problems of biological toxicity, cell membrane translocation and their complicated fabrication. To date, iodinated small molecules are still the most widely used clinical CT contrast agents because of their relative safety and well-established protocols for use. It is therefore highly meaningful to develop new smart iodinated CT contrast agents that can be specifically triggered to form nanoparticles in the tumour microenvironment so as to improve their accumulation and retention in tumours for high-performance CT imaging *in vivo*.

Herein we have designed and developed a new smart acidic pH/reduction dual-stimuli responsive nanoprobe that can specifically form intracellular aggregates under the stimulation of acidic pH and GSH conditions in the tumour microenvironment (Scheme 1). When probe **1** reaches cancer cells, the release of a citraconic motif is triggered by endosomal

[a]*State Key Laboratory of Radiation Medicine and Protection, School for Radiological and Interdisciplinary Sciences (RAD-X) and Collaborative Innovation Centre of Radiation Medicine of Jiangsu Higher Education Institutions, Soochow University, 199 Renai Road, Suzhou 215123, China. E-mail: hbshi@suda.edu.cn*
[b]*Key Laboratory of Organic Synthesis of Jiangsu Province, College of Chemistry, Chemical Engineering and Materials Science & Collaborative Innovation Center of Suzhou Nano Science and Technology, Soochow University, Suzhou 215123, P. R. China*
[c]*Department of Chemistry and Chemical Engineering, Jining University, Qufu 273155, China*
[d]*Department of Nuclear Medicine, Nanjing Medical University, Affiliated Wuxi People's Hospital, Wuxi, Jiangsu 214023, China*
†Electronic supplementary information (ESI) available. See DOI: 10.1039/c8nr05061a
‡These authors contributed equally to this work.

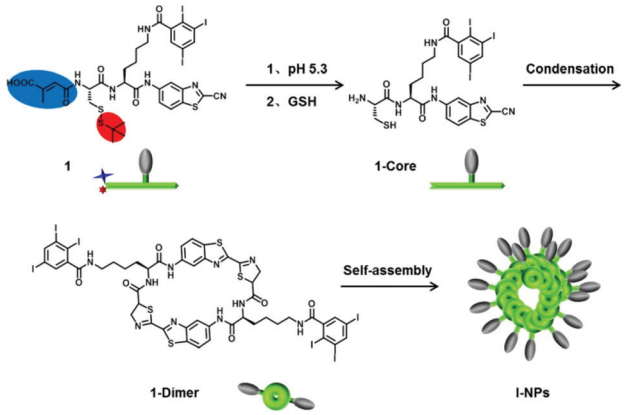

Scheme 1 Schematic illustration of a dually pH/GSH-controlled condensation and self-assembly of **I-NPs**.

acidic pH, and the disulfide bond of cysteine (Cys) is simultaneously reduced by intracellular GSH which is generally found at elevated levels in tumours,[16] resulting in the active intermediate (**1-Core**). The condensation of two **1-Core** spontaneously occurs by the well-known CBT condensation reaction developed by Rao[17] and Liang[18] between the cyano group of CBT and the 1,2-aminothiol group of Cys to yield the amphiphilic dimer (**1-Dimer**) that can *in situ* self-assemble into nanoparticles **I-NPs** *via* π–π stacking among each other, which prevents themselves from being pumped out by the cells, leading to improved accumulation and longer retention time of **I-NPs** in cancer cells. This acidic pH/GSH dual-mediated aggregation approach may provide a valuable tool to achieve enhanced CT imaging for precise diagnosis of tumours *in vivo*.

The study began with the synthesis of the active probe (**1**) and the control compound (**1-Scr**) (Fig. 1a). Both compounds were constructed with a triiodobenzoic group, 2-cyanobenzothiazole (CBT), and the caged Cys moiety linked through a lysine amino acid according to the synthetic route shown in Scheme S1 in the ESI.† The chemical structures of the intermediates and the desired products were verified by mass spectrometry (MS) and ^{1}H and ^{13}C NMR (Fig. S1–S18, ESI†). In addition, high performance liquid chromatography (HPLC) analysis reveals that probe **1** has good stability in phosphate-buffered saline (PBS, pH 7.0) and fetal bovine serum (FBS) aqueous solutions for 8 days (Fig. S19†).

To validate the occurrence of dually pH/GSH-mediated condensation and self-assembly, HPLC profiling analysis was firstly carried out to monitor the reaction of probe **1** after treatments with both acidic buffer and GSH. As shown in Fig. 1b, after 4 h of incubation of probe **1** (20 μM) in PBS buffer (pH 5.3) at 37 °C, only one peak on the HPLC trace at a retention time of 8.51 min (compound **2** in the ESI†) was determined. After checking by matrix assisted laser desorption ionization-time of flight mass spectrometry (MALDI-TOF MS), it was found that the citraconic moiety in **1** was hydrolysed under acidic conditions to afford an amine group (Fig. S20a†). The above reaction mixture was incubated with 10 mM GSH for a further 2 h, and then analyzed by HPLC and MS, respectively. One small peak on the HPLC trace of 5.89 min was identified as the active intermediate (**1-Core**), indicating that the disulfide bond of the Cys moiety of **1** can be reduced by GSH (Fig. S20b†). Additionally, peaks at retention times of 6.19 min (**1-D-1**) and 7.64 min (**1-D-2**) shared an identical molecular weight and were identified as the diastereoisomers of the condensation products **1-Dimer** (Fig. S21†).

To characterize the aggregation of **I-NPs**, transmission electron microscopy (TEM) was firstly performed for probe **1** before and after CBT condensation. As shown in Fig. 1c and 2a, the average size of the nanoparticle aggregates is

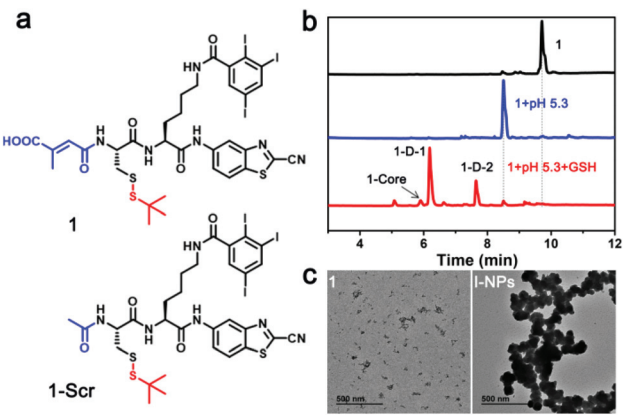

Fig. 1 (a) Chemical structures of **1** and its negative control **1-Scr**. (b) HPLC analysis of **1** (black); HPLC trace of the incubation mixture of **1** (20 μM) in PBS buffer (pH 5.3) at 37 °C for 4 h (blue); HPLC trace of the incubation mixture of **1** and GSH (10 mM) in PBS buffer (pH 5.3) at 37 °C for 2 h (red). Absorbance: 350 nm. (c) TEM images of **1** (left) and **I-NPs** (right).

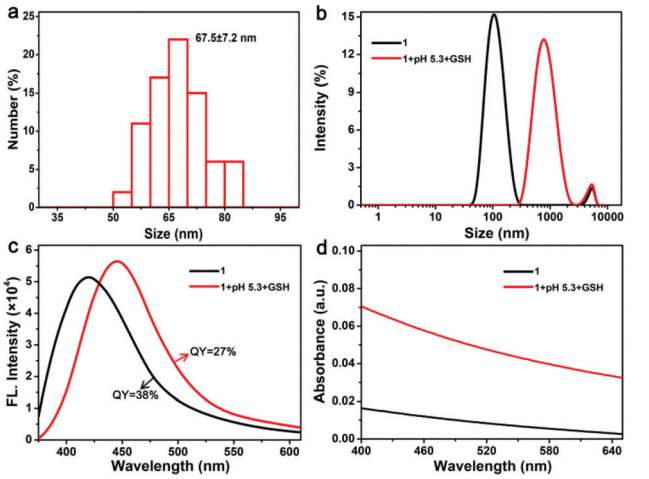

Fig. 2 (a) Statistical results of the diameters of nanoparticles in the TEM images of **I-NPs**. (b) Size distribution of **1** (black) and self-assembled **I-NPs** (red) measured by DLS. (c) Fluorescence emission of **1** (20 μM) before (black) and after CBT condensation (red). (d) Absorption spectra (400–650 nm due to the light scattering) of **1** at 20 μM before (black) and after condensation (red).

67.5 ± 7.2 nm after condensation. However, some amorphous deposition was only observed for **1** without condensation. Dynamic light scattering (DLS) was further carried out to monitor the variation of the hydrodynamic size of the probe before and after condensation. The hydrodynamic size of initial **1** was around 105 nm, while that of the resulting nanoparticles after condensation became 825 nm (Fig. 2b), highly suggesting the formation of a self-assembly of **I-NPs**. The fluorescence spectra of the above reaction mixture showed a red shift of the maximum from 420 to 445 nm in comparison with that of the solution of **1** (Fig. 2c), suggesting the formation of the cyclized dimer after condensation. The quantum yields of **1** and **1-NPs** in methanol were measured and calculated to be 38% and 27%, respectively (Fig. S22†). In addition, the UV-Vis spectra of the reaction mixtures at 400–650 nm presented a distinct increase of absorbance compared with that of the solution of **1** alone, which is attributed to the mono-dispersion of **I-NPs** after self-assembly (Fig. 2d). These results strongly suggest that probe **1** can be triggered to self-assemble into nanoparticles under acidic and reductive conditions.

The cytotoxicity of **1** and **1-Scr** was assessed through the widely used MTT (3-(4,5-dimethylthiazol-2-yl)-2,5-diphenyltetrazolium bromide) assays. As shown in Fig. S23,† probe **1** and **1-Scr** exhibit negligible cytotoxicity to the mouse fibroblast cell line 3T3 and murine breast carcinoma 4T1 cells below 60 μM. The overall cell viability for these two types of cells remained above 75% after 24 h of incubation. To investigate the potential of the dually pH/GSH-mediated condensation and self-assembly of **1** for enhancing cellular uptake, confocal laser scanning microscopy (CLSM) was adopted to image 4T1 living cells treated with the same concentration of **1** and **1-Scr**. The images were taken under excitation at 405 nm with a 430–480 nm band-pass filter. A weak fluorescence signal was observed from the control group of cells with **1-Scr** treatment. In contrast, strong blue fluorescence was obtained from the cells treated with **1** up to 4 h (Fig. 3), indicating that the cellular uptake and retention of **1** in 4T1 are obviously higher than those of **1-Scr**. These results highly support that the dually acidic pH/GSH-mediated condensation and self-assembly can greatly enhance the cellular uptake of **1** in cancer cells.

To further assess the possibility of using **1** as a specific bioprobe for *in vitro* cancer cell imaging, CLSM imaging was performed for both 4T1 and 3T3 cells. A commercial lysosome tracker was used to visualize the location of the cell lysosome. The images were taken under excitation at 405 nm with a 430–480 nm band-pass filter for the probe and at 559 nm with a 570–670 nm band-pass filter for the lysosome tracker. Fig. 4 presents the CLSM images of 4T1 and 3T3 live cells after incubation with **1** for 2 h. Apparently, the 3T3 cells exhibit extremely low fluorescence. In sharp contrast, under identical experimental conditions, strong fluorescence signals were obtained from 4T1 cancer cells. The signals can be greatly reduced when the cells were pretreated with diethylmaleate (DEM), a commercial GSH depletor, before incubation with **1**. Furthermore, excellent overlap is observed between the fluorescence images of the probe and lysosome tracker, suggesting that the probe mainly locates at the cell lysosome, which may be due to its acidic conditions. Collectively, all the above results firmly demonstrate that probe **1** can potentially be used for specific detection of cancer cells.

Iodinated organic compounds have usually been employed as the CT imaging agents due to the high-*Z* element iodine. The potential application of probe **1** as a targeted CT contrast agent in CT imaging was further evaluated. The *in vitro* CT images of **1**, **1-Scr** and a widely used clinical CT contrast agent (iopromide) were obtained and their CT values were measured by using a CT imaging system (MILabs, Utrecht, The Netherlands). As shown in Fig. 5a, the CT images of **1** and **1-Scr** have similar intensities with iopromide at equivalent concentrations, revealing their good potential for CT enhancement. Furthermore, the quantitative CT value analysis indicated that all three contrast agents had a concentration-

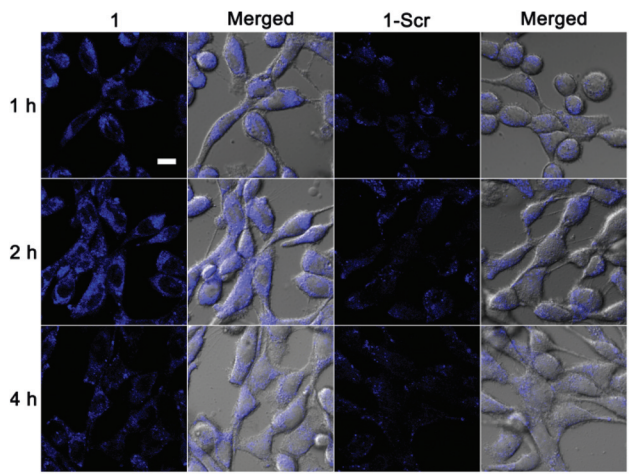

Fig. 3 CLSM images of 4T1 cells after incubation with 20 μM **1** and **1-Scr** at different time points. All images share the same scale bar (10 μm).

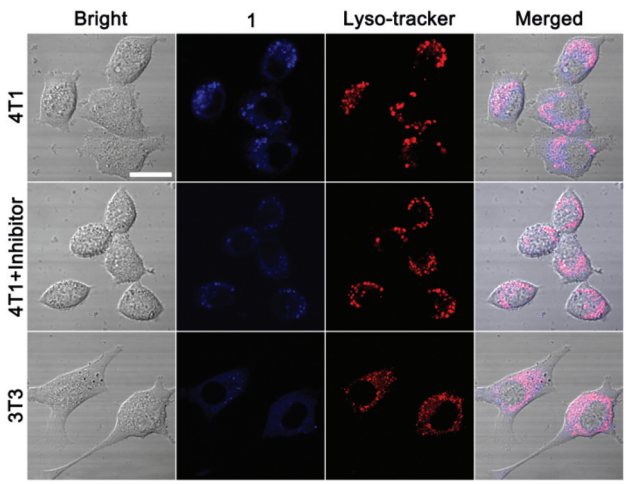

Fig. 4 Confocal imaging of 4T1 cells (top), 4T1 cells pretreated with DEM (diethylmaleate, 50 μM) (middle), and 3T3 cells (bottom) treated with **1** (20 μM) after 2 h of incubation, followed by staining with LysoTracker Red. The scale bar indicates 20 μm.

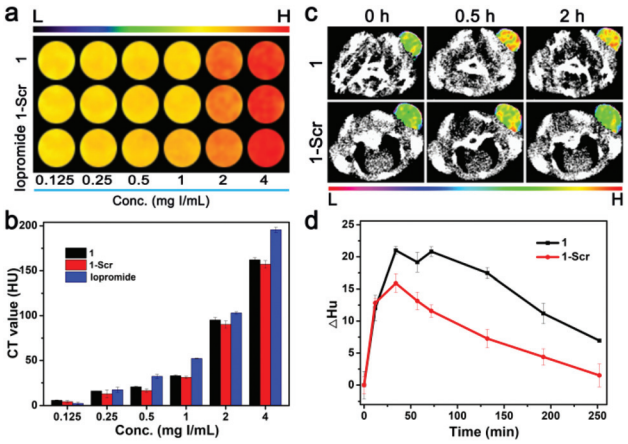

Fig. 5 (a) CT images of three series of aqueous solutions containing **1** (top), **1-Scr** (middle) and iopromide (bottom) with different concentrations, *i.e.*, 0.125, 0.25, 0.5, 1, 2 and 4 mg I per mL, respectively. (b) The quantified value in terms of HU of **1**, **1-Scr** and iopromide as functions of the concentrations. (c) CT imaging experiments of living mice with a subcutaneous 4T1 cell xenograft at 0 h, 0.5 h and 2 h after intravenous injections of **1** (upper) or **1-Scr** (lower) *via* tail veins. (d) Dynamic contrast enhanced density (ΔHu) of tumour CT imaging at different time intervals.

dependent CT enhancement. At a concentration of 4 mg I per mL, the hounsfield unit (HU) values of **1**, **1-Scr** and iopromide were 162.09, 157.01 and 195.58 HU, respectively (Fig. 5b). These results highly suggest that probe **1** could be potentially used as a CT contrast agent to visualize the tumour *in vivo*.

To further evaluate the *in vivo* application potential, the body clearances of both probe **1** and iopromide in mice were firstly investigated by measuring the CT contrast change (ΔHu) of the bladder using a consecutive CT scanner over a period of 4 h after intravenous injection. The injected dose was 44.58 mg I per kg for both samples. Enhanced CT contrasts of both groups of mice were subsequently determined for bladders with increasing time. The mice with an injection of iopromide showed a significant CT signal increase in the bladder with the highest contrast change of 310 at 16 min post-injection, while a slow CT signal increase was observed for the mice receiving **1**. ΔHu was only 156 at 4 h post-injection (Fig. S24†), which is ascribed to the long blood circulation of probe **1** nanoparticles (Fig. S25†). All these pieces of evidence suggest that iopromide has faster body clearance than probe **1**. Next, we also performed the CT imaging of tumours *in vivo*. 200 μL of an aqueous solution of **1** (5 mM) was intravenously injected into the tail vein of living female nude mice bearing 4T1 tumours, and subsequently the cross-sectional CT images of the tumours were recorded over time. Meanwhile, 4T1 tumour-bearing mice intravenously receiving 200 μL of an aqueous solution of **1-Scr** (5 mM) were set as the control group. Fig. 5c and Fig. S26† show a series of representative CT images of mice (n = 4) bearing 4T1 tumour xenografts acquired at selected time points after the intravenous injection of probe **1** or **1-Scr**. Clearly, enhanced CT contrasts of both groups of mice were observed for tumours with increasing time owing to the gradual homing of compounds at the tumour site. The quantitative analysis indicated that the highest contrast change (ΔHu) was up to 21 for mice injected with **1** at 0.5 h post-injection. In contrast, no significant tumour signals were recorded in the CT images of mice injected with **1-Scr**, and the highest ΔHu was only 15.91 at 0.5 h post-injection, which is probably due to the poor retention of **1-Scr** at the tumour site. Additionally, the tumour CT values of mice injected with probe **1** were always significantly higher than those of the **1-Scr** treated group. These results demonstrate that probe **1** has a better CT contrast performance than **1-Scr**. Besides, the CT signals from both groups of tumours gradually decreased after 0.5 h post-injection; the tumours receiving **1** at 4 h still retained 33.1% CT signals (ΔHu = 6.95) of that at 0.5 h (ΔHu = 21). However, it was only 9.5% (ΔHu = 1.52) for **1-Scr** (Fig. 5d), indicating that probe **1** exhibits prolonged retention time at the tumour site after CBT condensation. Collectively, all these results demonstrate that the dually acidic pH/GSH-mediated condensation and self-assembly of the probe enables one to dramatically improve the uptake and retention time of CT contrast agents in tumours.

In conclusion, we have successfully developed a novel smart dually acidic pH/GSH-responsive nanoprobe for enhanced CT imaging of tumours *in vivo*. Both *in vitro* and *in vivo* studies have demonstrated that probe **1** can be triggered by acidic pH and GSH to undergo intermolecular CBT condensation and form a nanoparticle assembly in the tumour microenvironment, which in consequence dramatically improves the cellular uptake and retention of the probe in tumours. We thus believe that the delicate dual stimuli-mediated assembly concept demonstrated herein may offer a promising theranostic tool for tumour treatment.

Conflicts of interest

The authors declare no conflicts of interest.

Acknowledgements

This work was financially supported by the National Key Research and Development Program of China (2016YFC0101200), the National Natural Science Foundation of China (21572153), the Key Research and Development Program of Social Development of Jiangsu Province (BE2018655), the Key Program of Natural Science Foundation of Jiangsu Educational Committee (15KJA310004), the Six Talent Peaks Project of Jiangsu Province (YY-032), and Suzhou Science and Technology Program (SYG201520).

Notes and references

1 (*a*) J. Condeelis and R. Weissleder, *Cold Spring Harbor Perspect. Biol.*, 2010, **2**, a003848; (*b*) T. Hussain and

Q. T. Nguyen, *Adv. Drug Delevery Rev.*, 2014, **66**, 90; (*c*) P. Mapelli and M. Picchio, *Nat. Rev. Urol.*, 2015, **12**, 510; (*d*) A. J. Shuhendler, K. Pu, L. Cui, J. P. Uetrecht and J. Rao, *Nat. Biotechnol.*, 2014, **32**, 373.

2 (*a*) S. Yang, D. Xing, Q. Zhou, L. Xiang and Y. Lao, *Med. Phys.*, 2007, **34**, 3294; (*b*) X. Wang, Y. Pang, G. Ku, X. Xie, G. Stoica and L. V. Wang, *Nat. Biotechnol.*, 2003, **21**, 803; (*c*) N. R. Evans, J. M. Tarkin, J. R. Buscombe, H. S. Markus, J. H. F. Rudd and E. A. Warburton, *Nat. Rev. Neurol.*, 2017, **13**, 676.

3 (*a*) J. R. Lindner and A. Sinusas, *J. Nucl. Cardiol.*, 2013, **20**, 990; (*b*) L. W. Dobrucki and A. J. Sinusas, *Nat. Rev. Cardiol.*, 2009, **7**, 38.

4 (*a*) M. Baker, *Nature*, 2010, **463**, 977; (*b*) B. R. Smith and S. S. Gambhir, *Chem. Rev.*, 2017, **117**, 901; (*c*) M. Rudin and R. Weissleder, *Nat. Rev. Drug Discovery*, 2003, **2**, 123; (*d*) Q. Miao and K. Pu, *Bioconjugate Chem.*, 2016, **27**, 2808; (*e*) H. Zhu, Y. Fang, X. Zhen, N. Wei, Y. Gao, K. Q. Luo, C. Xu, H. Duan, D. Ding, P. Chen and K. Pu, *Chem. Sci.*, 2016, **7**, 5118.

5 (*a*) X. Pan, J. Siewerdsen, P. La Riviere and W. Kalender, *Med. Phys.*, 2008, **35**, 3728; (*b*) H. Lusic and M. W. Grinstaff, *Chem. Rev.*, 2013, **113**, 1641; (*c*) L. Schenkman, *Science*, 2011, **331**, 1002.

6 (*a*) J. Kim, P. Chhour, J. Hsu, H. I. Litt, V. A. Ferrari, R. Popovtzer and D. P. Cormode, *Bioconjugate Chem.*, 2017, **28**, 1581; (*b*) L. Nohyun, C. S. Hong and H. Taeghwan, *Adv. Mater.*, 2013, **25**, 2641.

7 Y. Liu, K. Ai and L. Lu, *Acc. Chem. Res.*, 2012, **45**, 1817.

8 J. Singh and A. Daftary, *J. Nucl. Med. Technol.*, 2008, **36**, 69.

9 (*a*) X. Li, N. Anton, G. Zuber, M. Zhao, N. Messaddeq, F. Hallouard, H. Fessi and T. F. Vandamme, *Biomaterials*, 2013, **34**, 481; (*b*) J. Ding, Y. Wang, M. Ma, Y. Zhang, S. Lu, Y. Jiang, C. Qi, S. Luo, G. Dong, S. Wen, Y. An and N. Gu, *Biomaterials*, 2013, **34**, 209; (*c*) Y. Zou, Y. H. Wei, G. L. Wang, F. H. Meng, M. Y. Gao, G. Storm and Z. Y. Zhong, *Adv. Mater.*, 2017, **29**, 1603997; (*d*) H. Zhu, Y. Fang, Q. Miao, X. Qi, D. Ding, P. Chen and K. Pu, *ACS Nano*, 2017, **11**, 8998.

10 (*a*) X. Li, N. Anton, G. Zuber and T. Vandamme, *Adv. Drug Delevery Rev.*, 2014, **76**, 116; (*b*) C.-Y. Kao, E. A. Hoffman, K. C. Beck, R. V. Bellamkonda and A. V. Annapragada, *Acad. Radiol.*, 2003, **10**, 475; (*c*) S. Mukundan, K. B. Ghaghada, C. T. Badea, C.-Y. Kao, L. W. Hedlund, J. M. Provenzale, G. A. Johnson, E. Chen, R. V. Bellamkonda and A. Annapragada, *Am. J. Roentgenol.*, 2006, **186**, 300.

11 (*a*) S. You, H.-Y. Jung, C. Lee, Y. H. Choe, J. Y. Heo, G.-T. Gang, S.-K. Byun, W. K. Kim, C.-H. Lee, D.-E. Kim, Y. I. Kim and Y. Kim, *J. Controlled Release*, 2016, **226**, 258; (*b*) Q. Yin, F. Y. Yap, L. Yin, L. Ma, Q. Zhou, L. W. Dobrucki, T. M. Fan, R. C. Gaba and J. Cheng, *J. Am. Chem. Soc.*, 2013, **135**, 13620; (*c*) C. Xie, X. Zhen, Q. Lei, R. Ni and K. Pu, *Adv. Funct. Mater.*, 2017, **27**, 1605397.

12 (*a*) M. Chen, S. Tang, Z. Guo, X. Wang, S. Mo, X. Huang, G. Liu and N. Zheng, *Adv. Mater.*, 2014, **26**, 8210; (*b*) A. Al Zaki, D. Joh, Z. Cheng, A. L. B. De Barros, G. Kao, J. Dorsey and A. Tsourkas, *ACS Nano*, 2014, **8**, 104; (*c*) X. Cheng, R. Sun, L. Yin, Z. Chai, H. Shi, M. Gao and M. Y, *Adv. Mater.*, 2017, **29**, 201604894; (*d*) Y. Yu, Y. Wu, J. Liu, Y. Liu and D. Wu, *Nanoscale*, 2017, **9**, 9447.

13 Y. Jin, Y. Li, X. Ma, Z. Zha, L. Shi, J. Tian and Z. Dai, *Biomaterials*, 2014, **35**, 5795.

14 L. Wang, H. Xing, S. Zhang, Q. Ren, L. Pan, K. Zhang, W. Bu, X. Zheng, L. Zhou, W. Peng, Y. Hua and J. Shi, *Biomaterials*, 2013, **34**, 3390.

15 (*a*) J. Liu, X. Zheng, L. Yan, L. Zhou, G. Tian, W. Yin, L. Wang, Y. Liu, Z. Hu, Z. Gu, C. Chen and Y. Zhao, *ACS Nano*, 2015, **9**, 696; (*b*) G. Song, C. Liang, H. Gong, M. Li, X. Zheng, L. Cheng, K. Yang, X. Jiang and Z. Liu, *Adv. Mater.*, 2015, **27**, 6110; (*c*) F. Mao, L. Wen, C. Sun, S. Zhang, G. Wang, J. Zeng, Y. Wang, J. Ma, M. Gao and Z. Li, *ACS Nano*, 2016, **10**, 11145; (*d*) Y. Li, Y. Sun, T. Cao, Q. Su, Z. Li, M. Huang, R. Ouyang, H. Chang, S. Zhang and Y. Miao, *Nanoscale*, 2017, **9**, 14375.

16 X. Jin, S. Kang, S. Tanaka and S. Park, *Angew. Chem., Int. Ed.*, 2016, **55**, 7939.

17 (*a*) G. Liang, H. Ren and J. Rao, *Nat. Chem.*, 2009, **2**, 54; (*b*) D. Ye, G. Liang, M. L. Ma and J. Rao, *Angew. Chem., Int. Ed.*, 2011, **50**, 2275.

18 (*a*) Z. Zheng, P. Chen, M. Xie, C. Wu, Y. Luo, W. Wang, J. Jiang and G. Liang, *J. Am. Chem. Soc.*, 2016, **138**, 11128; (*b*) Y. Yuan and G. Liang, *Org. Biomol. Chem.*, 2014, **12**, 865; (*c*) X. Liu and G. Liang, *Chem. Commun.*, 2017, **53**, 1037; (*d*) Y. Yuan, D. Li, J. Zhang, X. Chen, C. Zhang, Z. Ding, L. Wang, X. Zhang, J. Yuan, Y. Li, Y. Kang and G. Liang, *Chem. Sci.*, 2015, **6**, 6425.

